Acta Biomaterialia 169 (2023) 542–555

Contents lists available at ScienceDirect

Acta Biomaterialia

journal homepage: www.elsevier.com/locate/actbio

Full length article

Tracking adoptive natural killer cells via ultrasound imaging assisted with nanobubbles

Yizhou Jiang, Xuandi Hou, Xinyi Zhao, Jianing Jing, Lei Sun*

Department of Biomedical Engineering, The Hong Kong Polytechnic University, Room ST409 Hung Hom, Hong Kong SAR 999077, PR China

ARTICLE INFO

Article history:
Received 4 May 2023
Revised 6 July 2023
Accepted 27 July 2023
Available online 1 August 2023

Keywords:
Cell tracking
Cell therapy
Immunotherapy
Ultrasound imaging
Nanobubbles

ABSTRACT

The recent years has witnessed an exponential growth in the field of natural killer (NK) cell-based immunotherapy for cancer treatment. As a prerequisite to precise evaluations and on-demand interventions, the noninvasive tracking of adoptive NK cells plays a crucial role not only in post-treatment monitoring, but also in offering opportunities for preclinical studies on therapy optimizations. Here, we describe an NK cell tracking strategy for cancer immunotherapy based on ultrasound imaging modality. Nanosized ultrasound contrast agents, gas vesicles (GVs), were surface-functionalized to label NK cells. Unlike traditional microbubble contrast agents, nanosized GVs with their unique thermodynamical stability enable the detection of labeled NK cells under nonlinear contrast-enhanced ultrasound (nCEUS), without a noticeable impact on cellular viability or migration. By such labeling, we were able to monitor the trafficking of systematically infused NK cells to a subcutaneous tumor model. Upon co-treatment with interleukin (IL)-2, we observed a rapid enhancement in NK cell trafficking at the tumor site as early as 3 h post-infusion. Altogether, we show that the proposed ultrasound-based tracking strategy is able to capture the dynamical changes of cell trafficking in NK cell-based immunotherapy, providing referencing information for early-phase monotherapy evaluation, as well as understanding the effects of modulatory co-treatment.

Statement of significance

In cellular immunotherapies, the post-infusion monitoring of the living therapeutics has been challenging. Several popular imaging modalities have been explored the monitoring of the adoptive immune cells, evaluating their trafficking and accumulation in the tumor. Here we demonstrated, for the first time, the ultrasound imaging-based immune cell tracking strategy. We showed that the acoustic labeling of adoptive immune cells was feasible with nanosized ultrasound contrast agents, overcoming the size and stability limitations of traditional microbubbles, enabling dynamical tracking of adoptive natural killer cells in both monotherapy and synergic treatment with cytokines. This article introduced the cost-effective and ubiquitous ultrasound imaging modality into the field of cellular immunotherapies, with broad prospectives in early assessment and on-demand image-guided interventions.

1. Introduction

Adoptive cell therapy (ACT), a type of cell-based immunotherapeutic approach, has provided tremendous opportunities for cancer treatment and management in recent years [1–3]. In ACT, *ex vivo*-expanded effector immune cells, either autologous or allogenic, are adoptively infused into patients for the treatment of cancers, which has shown promising outcomes in leukemia and lymphoma patients [1,2]. Despite the encouraging success of ACT in various aspects, challenges remain as many patients failed to respond or underwent relapse after the treatment, with widely reported heterogeneity in intratumoral recruitment of the therapeutic cells and sometimes off-tumor toxicity [4–8]. In recent years, natural killer (NK) cells have emerged as an attractive candidate in cell-based immunotherapies. These innate effector cells, with ease of access and expansion, feature a direct cytotoxicity against cancer cells even in case of tumor antigen loss, making them a promising alternative for non-responders to adoptive T cell therapies. Their presence in the tumor sections have been widely reported to posi-

* Corresponding author.
E-mail address: lei.sun@polyu.edu.hk (L. Sun).

https://doi.org/10.1016/j.actbio.2023.07.058

tively correlate with treatment responses, with better safety profile after adoptive transfer, encouraging increasing efforts on developing NK-based immunotherapies in both preclinical and clinical settings [9–11].

With the advances in the cancer-immune biology, there is a growing awareness of the importance of tracking these adoptive immune cells after the transfer. The trafficking, infiltration, persistence and anti-tumor activities of these infused immune cells in tumor microenvironment (TME), etc., reflect crucial information for the post-treatment assessment as well as the development of adjuvant strategies for the full exploitation of their therapeutic effects [12,13]. As a prerequisite to precise interventions and modulations, tracking the adoptive NK cell accumulation in the tumor also provides opportunities for designs of on-target activation strategies to increase the specificity and safety. This poses substantial challenges to traditional follow-up examinations like blood tests or biopsies, which are suggested to suffer from limited spatial information and delayed identification of insufficient tumor recruitment of the adoptive cells. By contrast, with the imaging-based noninvasive cell tracking techniques, the tumor recruitment, retention and even activation status of the adoptive NK cells could be assessed with spatial precision, enabling early evaluation of the treatment and informed treatment-related decision making [7,12,14–18]. The recent years have seen tremendous efforts in exploring effective imaging strategies, with combinations of advanced materials, to enable therapeutic cell tracking. Various modalities have been explored for the tracking of adoptive cells, including optical imaging methods, nuclear medicine imaging and magnetic resonance imaging [15,19–23]. Different modalities have been contributing new insights of adoptive cells to the field with their unique advantages, serving as powerful post-infusion monitoring tools either in preclinical settings or with clinical relations. Yet, none of these methods has been deemed as the gold-standard, having their own limitations.

The ultrasound imaging, as a cost-effective, radiation-free, widely accessible and sensitive technique, enjoys not only the deep penetration, but also the capability of real-time imaging at the same time. It has been routinely used for imaging examinations and image-guided procedures in clinical practices, including administration of therapeutic immune cells, making it another attractive modality for tracking cells in ACT. However, there has been limited results on ultrasound imaging for the cell tracking purposes, especially in cell-based immunotherapies. To achieve ultrasound imaging of a target cell population, the ultrasound contrast agents (UCAs) are needed for enhancing the signal contrast from cells of interests, making them distinguishable from surrounding tissues. Microbubbles (MBs), either lipid- or protein-shelled, are the most commonly used UCAs, with many commercially available formulations [24,25]. The immune cells of interests are expected to migrate and infiltrate into tumor tissues, thus the tracking of which requires the cell-bound UCAs to have sizes smaller than the particle passing limits in tumors [26]. Unfortunately, MBs, with their micron-scale sizes, are usually confined to the vasculature and hence are limited for the cell tracking purposes. Moreover, the MBs are thermodynamically unstable at *in vivo* conditions, with documented rapid signal decay under body temperature (37°C), while the dynamics of adoptive immune cells like NK cells could be beyond the lifetime of MBs [25,27,28]. If the tracking of adoptive NK cells could be implemented by the already-on board ultrasound imaging technology, assisted by nanosized UCAs with better stability, the early and cost-effective monitoring of these therapeutic cells will be possible, as well as the image-guided interventions on adoptive cells.

For the tracking of adoptive NK cells with ultrasound, it is desired to employ UCAs with smaller sizes and better *in vivo* stability. Gas vesicles (GVs) are biogenic protein-shelled hollow structures with nanoscale sizes, which have been demonstrated as genetically encodable ultrasound contrast agents with tremendous potentials in various fields [29,30]. These structures are mechanistically stable as the protein shells exclude water and allow free gas exchange between the surrounding media, providing a desired thermodynamical stability for *in vivo* persistence. It has been demonstrated that the flexible shells of GVs buckle under acoustic field, generating echo in the harmonic frequencies, allowing the distinguishment of GVs from biological tissues with echo dominantly in fundamental frequency [31–33]. Their role of gas-carrying oscillators under ultrasound activation has been exploited for therapeutic purposes, as well as site-specific neuromodulation [34–36]. The nonlinear echogenicity of GVs has also been exploited for nonlinear contrast-enhanced ultrasound (nCEUS) imaging. Thanks to recent advances in the field, it has been demonstrated to be effective reporters in GV-expressing cells for imaging purposes, as well as modifiable nanosized contrast agents for molecular ultrasound imaging [37–41].

Herein, we hypothesize that GVs could be sued as acoustic markers to label NK cells, which in turns enables noninvasive tracking of the labeled cells after systematic infusion via ultrasound imaging. We chose NK-92 cells, an off-the-shell NK cell line with great translational potentials, as example cells for tracking . In a model system of adoptive NK cell immunotherapy, we showed that the GV-based labeling allows ultrasound imaging of labeled NK-92 cells during their trafficking to the tumor xenograft of human hepatocellular carcinoma. We found that the labeled NK cells accumulated within the tumor as early as 3 h after the adoptive infusion, which led to a significant increase in the signal intensity under nCEUS imaging. We further showed that, upon actively boosting the NK-cell tumor accumulation by the well-recognized booster IL-2, the ultrasound signal drastically increased at both 3 h and 24 h post-infusion. The increased tumor recruitment of adoptive NK cells could also be confirmed by *ex vivo* optical imaging techniques, suggesting the successful noninvasive tracking of the adoptive NK cells by the proposed method.

2. Materials and method

2.1. GV preparation

2.1.1. GV extraction

The GVs were extracted from *Anabaena flos-aquae* by Walsby's method (Buckland and Walsby, 1971). Briefly, the hypertonic cell lysis was used isolate GVs from *Ana* by suspending the cells in 25% sucrose solution and standing the resulting mixture in 4 °C overnight. The released GVs floated to the top were collected and purified with PBS by centrifugation-assisted floatation. The infranatant was removed by 20G needles and the floating GVs at top were resuspended in PBS. The purification procedures were repeated until the GVs formed a creamy white layer on top of clear infranatant. Finally, the GVs were stored in PBS at 4 °C.

2.1.2. GV characterization

For the characterization of GV size distribution and zeta potential, the Zetasizer Nano-Z (Malvern Instruments Ltd, Malvern, UK) was used. The GVs were suspended in DI water according to manufacturer's instruction with temperature balanced to 25 °C during the measurement. The concentration of GVs was determined using UV-Vis spectrometer (100 Pro, GE Healthcare, USA) as previously described [34–36,39], where a documented concentration of $450pM/OD_{500nm}$ was adopted in the measurement.

2.1.3. GV functionalization

To functionalize GVs for binding with cells through the biotin-streptavidin interaction, the GV surface proteins were first bi-

otinylated with EZ-Link Sulfo-NHS-Biotin (ThermoFisher Scientific) according to the supplier's instructions. Briefly, the biotinylation reagent was added to purified GVs with a 10000-fold molar excess at 2mM concentration. Following a 20 min incubation at room temperature, the biotinylated GVs were washed with PBS 3 times through centrifugal floatation. The biotinylated GVs were further mixed with Dylight594-conjugated streptavidin at molar ratio of 1:10000 and incubated for 30 min at room temperature, in order to form non-aggregated GVs with streptavidin-functionalized surfaces and detectable with fluorescence imaging. The resulting streptavidin-coated GVs (SA-GVs) were further washed and purified 3 times with PBS to get rid of non-incorporated reagents and stored in PBS at 4°C before further use. The size distribution of functionalized GVs was characterized by dynamic light scattering (DLS) method as the plain GVs, where no significant shift of the size was observed.

2.2. Cell labeling with GVs

2.2.1. NK cell culture

The human NK cell line, NK-92, was obtained from American Type Culture Collection (Rockville, MD, USA), and cultured at 37°C with 5% CO_2, in MEM-α medium (12561056, ThermoFisher Scientific), supplemented with 10% heat-inactivated FBS, 1% penicillin/streptomycin, 100U/mL IL-2, 0.02mM folic acid, 0.2mM inositol, and 0.1mM 2-Mercaptoethanol. To facilitate the confirmation of GV binding and also co-validation of the biodistribution by optical imaging methods, the NK cells were transfected with EGFP reporter gene and sorted on the basis of EGFP expression before further experiments. The Hep-3B cell line was obtained from ATCC and cultured in DMEM medium, supplemented with 10% FBS and 1% penicillin/streptomycin.

2.2.2. Labeling of biotinylated NKs

To attach SA-GVs to NK cells, the cell surface was biotinylated with EZ-Link Sulfo-NHS-Biotin (ThermoFisher Scientific), using procedures similar to the GV biotinylation described above. The reaction mixture of cells and the reagent was incubated at 4°C according to supplier's suggestions to avoid active internalization of biotin during the process. The cells were washed with PBS 3 times after the biotinylation process to get rid of the non-incorporated biotin reagents. For the binding between SA-GVs and biotinylated NK cells, the mixture of 80μL SA-GVs (OD10 in PBS) and cell suspension of 5×10^7 cells in PBS was incubated at 4 °C for 30 min. Gentle shaking was applied with the orbital shaking bed to avoid cell pelleting during the incubation which might result in GV-bridged cell-cell binding. The resultant suspension was further washed 3 times with ice-cold PBS, where the supernatant that contained unbound free GVs was removed. The dosage of GVs for current labeling procedures was empirically determined through several trials, where the 100% labeling rate (ratio of cells that exhibited GV-related signal in fluorescence imaging) was achieved without introducing cell floatation due to binding with large amount of GVs, whereas the GV-cell ratio was high enough to prevent GV-bridged cell-cell binding.

To compare the influence of different UCAs on cell migration, MB-labeled cells were prepared with similar procedures. The streptavidin-coated MBs were prepared by first synthesizing biotin-coated MBs. Then similar streptavidin coating procedures like GVs were applied. To exclude the potential bioeffect of MB lipid components on cell migration, another labeling group with ruptured MBs was included. The same number of bubbles as in MB-labeling group was used during labeling, except for the bubbles in this group were pretreated by sonication bath to shatter the bubbles and release their shell components.

2.3. Cell viability and functionality tests

2.3.1. MTS test

The impact of different labeling agents on NK cell viability was examined with 3-(4,5-dimethylthiazol-2-yl)-5-(3-carboxymethoxyphenyl)-2-(4-sulfophenyl)-2H-tetrazolium (MTS) assay. The NK cells were bound with either GVs or MBs through the biotin-avidin interactions described above, and the viability was compared to a control group where no labeling agent was added (CTRL). After the labeling procedures, the cells were seeded in 96-well plates at 5×10^3 cells/well incubated for each of the groups. The cells were incubated for 0, 24, 48, and 72 h before adding 10μL MTS, followed by an extra 3 h incubation to allow the reaction of the reagent. Afterwards, the absorbance at 492 nm was measured with a microplate reader (Ledetect 96, Labexim Products, Austria).

2.3.2. Migration test

The influence of different labeling agents on NK cell migration ability was examined by transwell tests. Apart from the binding with GVs and MBs, an additional labeling group of shattered MBs (MB-S) was included to exclude potential bioeffects of MB shell components on the migration ability. After cell labeling procedures, the cells were resuspended in FBS- culture medium, with cell densities balanced to 10^6/mL in each group. Then 100μL of the cell suspension was seeded into the transwell inserts (5μm pore size) of 24-well Transwell (Corning Inc., Corning, NY), resulting in a final cell number of 10^5 in each insert. The bottom chamber was added with 600μL full medium to attract the migration of NK cells. After a 24 h incubation, the medium at the bottom chamber was collected for counting migrated cells through the pores.

2.4. In vitro *ultrasound imaging*

The *in vitro* ultrasound imaging properties of GV-labeled NK cells were evaluated in a custom-made 3% (w/v) agarose phantom. Briefly, the agarose was dissolved in Milli-Q water by heating, and the hot solution was solidified in a custom-made mold. A pipet tip was inserted to the hot solution from the top before solidification, so that a sample loading well was formed in the phantom. The suspensions of either unlabeled or GV-labeled NK cells were loaded into the phantom well and imaged with the Vevo 2100 imaging system (Visual Sonics, Fujifilm, Toronto, Canada). The LZ250 transducer operating at 18MHz was used for acquiring the nonlinear contrast mode images (Transmit Power 4%, Standard Beamwidth, Contrast Gain 30dB, Dynamic Range 30dB). To confirm the nonlinear contrast signal was indeed coming from intact GVs bound with cells, a high-power ultrasound burst (Transmit Power 100%, Duration 1 second) was applied on the sample suspension to see whether the contrast would be eliminated.

To understand the detection sensitivity and signal persistence *in vitro* of current tracking strategy, the ultrasound imaging properties of labeled cells were first evaluated against cell densities and post-labeling incubation time *in vitro*. For density-dependent imaging properties, the cells were resuspended to several densities from 10^3 to 10^6 cells/mL after labeling procedures. For the incubation-time dependent evaluation, the labeled cells were resuspended in FBS-low (3%) medium and put to incubation at 37 °C, such that the cell proliferation would not complicate the evaluation of cell-bound GV stability. At different time points after the incubation (0, 24, 48 and 72 h), the sample was collected from the culture, pelleted and resuspended in PBS with density balanced to 10^6 cells/mL for imaging experiments. All *in vitro* imaging of the cells were then carried out in the phantom well at room temperature.

2.5. Animal experiments

All animal experiments were conducted under experiment protocols approved by Department of Health of Hong Kong SAR and the Hong Kong Polytechnic University Animal Subjects Ethics Subcommittee (Approval No. 20-21/250-BME-R-NSFC). Male nude mice of 5 weeks old, weighing 20∼24 g were provided by the Centralized Animal Facilities of Hong Kong Polytechnic University. The tumor xenograft was established by subcutaneously injection of 2×10^7 Hep-3B cells in full medium mixed 1:1 with Matrigel (100μL) to the right rear dorsum. The tumor started to be apparent about 2 weeks after the injection and the volume was measured by calipers and B-mode ultrasound imaging. The experiments started at the time point when tumors reached average sizes of 50∼100mm^3. The animals were randomly divided into 4 groups: (a) GV only, (b) NK only, (c) GVNK, (d) Control, corresponding to the intravenous injection of (a) 80μL GVs in PBS (OD10), (b) 5×10^6 NK cells in 80μL PBS, (c) 5×10^6 GV-labeled NK cells in 80μL PBS, and (d) 80μL PBS. The tumor growth was monitored in all groups, and the ultrasound imaging was conducted on mice in (a), (b) and (c) before and 3, 24, 48, 72 and 96 h after the injection. To further boost the tumor targeting ability of infused NK cells, another group (e) GVNK+IL2 was added, where the mice receive the same amount of labeled NK cells as in (c), while a single dose of recombinant IL-2 (50×10^3U) was injected i.p. at 1h after the NK cell infusion. The *in vivo* toxicity of the treatment and tracking system was monitored by the observations of the body weight, food intake and daily activity of the mice. One mouse from each of the three groups (NK only, GVNK and GVNK+IL2) was sacrificed at 24 h after the injection, and the tumors and major organs (heart, liver, spleen, kidney and lung) were collected for IVIS imaging (Perkin Elmer, Waltham, MA). The tumors were further fixed with 4% paraformaldehyde and slices were collected by cryosection for further fluorescence microscopy. The liver imaging experiments were conducted in another batch of healthy nude mice, divided into 3 groups receiving i.v. injection of either GVs, NK cells or GV-labeled NK cells. The liver contrast was evaluated every 15 min following the IV injection and the major organs were also collected for IVIS imaging.

For the *in vivo* ultrasound imaging, the Vevo 2100 imaging system with the LZ250 transducer was used for capturing images under nonlinear contrast mode. The parameters were set according to manufacturer's instructions to suppress tissue backgrounds *in vivo* (Frequency 18MHz, Transmit Power 4%, Narrow Beamwidth, Contrast Gain 20dB, Dynamic Range 30dB). The mice were anesthetized by isoflurane with body temperature maintained, breathing and heartbeat monitored using the heated imaging platform. For tumor imaging experiments, the motor-controlled 3D ultrasound scanning was conducted (step size 0.05 mm) to obtain the contrast profiles within the entire tumor.

2.6. Image analysis of ultrasound images

The ultrasound images were exported, and MATLAB (Mathworks) was used to quantify the intensity values in the nonlinear contrast (NLC) mode images. The regions of interest (ROIs) were manually defined to cover the intra-tumoral volumes while avoiding the tissue boundaries. The average NLC intensity within the ROI was extracted from every two frames through the 3D scans, and the overall average NLC intensity was averaged through the entire tumor volume. The overall intra-tumoral contrast signal after the adoptive transfer was normalized to the baseline value, obtained via a scan before infusion, and presented in dB values. The 3D reconstruction of the tumor volume and corresponding contrast coverage analysis was conducted using the Vevo LAB software, similarly with manually drawn ROIs.

2.7. Confocal microscopy

For the confocal microscopy of NK cells, the GV-labeled and control NK cells were first fixed with 4% PFA for 10 min. After fixing, the cells were washed with PBS and then stained with DAPI mounting medium before sealed with cover slips. The cells were then observed with a laser-scanning confocal microscope (Leica TCS SPE, Germany) with 40X objective. The NK cells were observed by 488nm laser excitation for their EGFP expression, while the GVs were visualized by the 561nm laser excitation for their surfaces coated with Dylight594. The processing and quantification of the obtained images was conducted using ImageJ software.

2.8. Transmission Electron Microscopy

To further determine the size and morphology of the prepared GVs, we used Transmission Electron Microscopy (TEM, JEOL 2100 F, JEOL, Tokyo, Japan) with an operating voltage of 200kV. The GV sample suspended in deionized water at OD0.1 was deposited on a carbon-coated formvar grid and let dried at room temperature before imaging.

2.9. Statistical analysis

The data was collected in triplicate unless stated otherwise, and all statistical analyses were conducted using MATLAB software. For comparisons between two groups, the two-tailed Student's t-test was used. The comparison among more than two groups was performed by one-way analysis of variance (ANOVA) followed by Fisher's least significant difference test for post-hoc correction. P-values lower than 0.05 were consider statistically significant. All statistical differences between groups were marked with corresponding p-values obtained in the analysis.

3. Results

3.1. GV binding on NK cells (with viability and migration)

To achieve ultrasound tracking of adoptive immune cells, we attached GVs as nanosized UCAs (nUCAs) on the cell surface through *ex vivo* biotin-streptavidin conjugation. After labeling, the labeled immune cells were systematically infused into tumor-bearing animals through i.v. injection. Upon infiltration and accumulation in the tumor, the cell bound GVs would exhibit specific ultrasound contrast, indicating the intra-tumoral homing of adoptive immune cells (Fig. 1a). The GVs were extracted and prepared according to previously determined protocols, where the ultrasound imaging properties and surface chemistry of GVs have also been well-characterized [30,35,36,39]. We have adopted surface-functionalized GVs in this study for the labeling of immune cells, without any additional modifications that shall be thought to alter their properties. For those who are interested in the detailed characteristics of these vesicles, one could refer to previous work that described the protocols we adopted. Indeed, the prepared GVs showed a cylindrical morphology with nanoscale dimensions, with no significant shift of size distribution after the surface functionalization (Fig. 1b, Supplementary Fig. S1). We then applied the prepared GVs for labeling surface biotinylated NK-92 cells *ex vivo* through biotin-streptavidin conjugation. As we used EGFP-expressing NK-92 cells as model targets, the binding between the fluorescence-labeled GVs and NK cells could be confirmed by fluorescence microscopy (Fig. 1c&d). Dylight594$^+$ spots could be observed with clustered distribution around EGFP signal, indicating a successful attachment of SA-GVs on the surfaces of biotinylated NK-92 cells (Fig. 1c). No GV-bridged cell-cell binding was observed under the current labeling protocol. From the images taken at

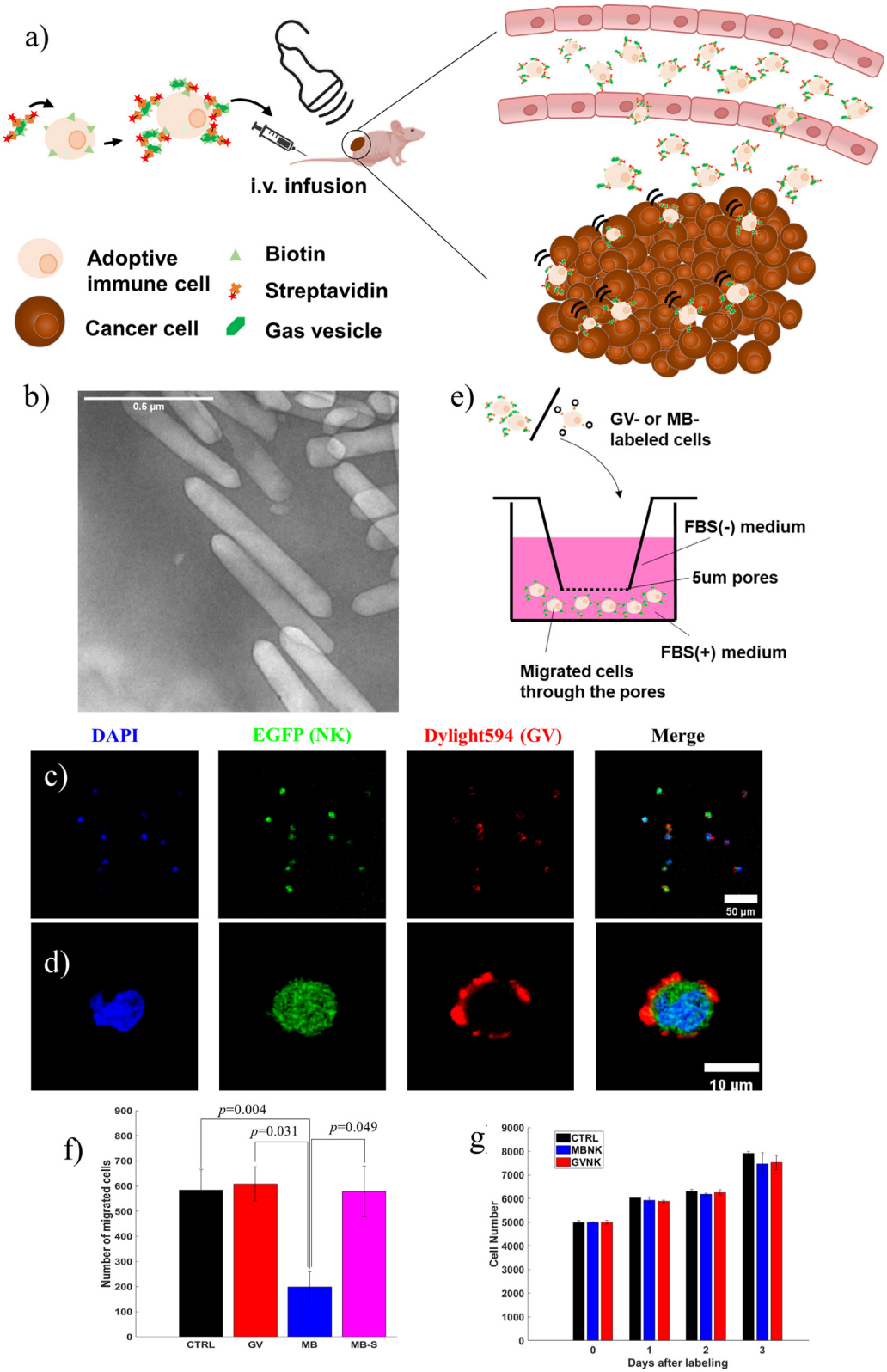

Fig. 1. GV-based labeling of adoptive immune cells and the tracking strategy. a. Schematic design of the *in vitro* labeling of adoptive immune cells with GVs via biotin-streptavidin interaction, which further grants the cells echogenicity for ultrasound imaging after systematic transfer. b. TEM image of GVs, indicating a cylindrical morphology with diameters around 100nm and length around 600nm . c, d. Fluorescence microscopy of GV-labeled NK-92 cells. The EGFP-expressing NK-92 cells (green) were labeled with Dylight594-conjugated GVs (red), with nucleus stained with DAPI (blue) and imaged with confocal microscopy at 10 × (c) and 40 × (d) objective lens. The merged images indicate that the cells were labeled with GVs without noticeable cell-to-cell binding, and the GVs were localized on the cell membrane after the labeling procedures. e. Schematic principle of the migration test. The GV- or MB- labeled cells were loaded into the transwell insert containing FBS-free medium, while the well contains full medium to attract the cells to migrate through the insert membrane with 5μm pores. An additional group of cells bound with shattered MBs (magenta) was also included in migration assay. f. The migrated cells at the well collected and counted for comparisons to control group (black). Statistical differences indicated with corresponding p-values. g. MTS assay on GV- (red) or MB- (blue) labeled cells with comparison to control (black). No significant impact of either contrast agents on cell proliferation observed ($n = 3$, data presented as mean ± SD).

higher magnification (Fig. 1d), the GVs were tethered to the cellular surfaces. By principle, the high labeling rate and the avoidance of cell-cell binding could be achieved with higher GV-to-cell ratio. While the overdose of GVs would result in cell floatation due to the strong buoyancy introduced by the large amount of GVs on the cells. This might impose difficulty in separating labeled cells from free GVs, also resulting in a potential barrier for cellular contact with cancer cells. Hence, all the experiments carried out in the current study were under the empirically determined GV dosage, with shaking applied during incubation. Note that the fluorescence intensity should be considered partially reflecting the loading capacity of GVs on each cell. The absolute red fluorescence intensity could also be related to variations in sizes of each GV, as well as attachment of GV shell fragments due to mechanical agitation applied during the mixing operations. Therefore, we only provided the fluorescence imaging for indication of successful surface attachment, instead of quantifying the number of intact GVs bound on each cell relying on the fluorescence. For the loading capacity of GVs on cells, one may find estimations via measuring the GV concentrations before and after the labeling procedures. The difference between starting GV dosage and the residual free GVs shall reflect the amount of GVs incorporated on labeled cell population (895 ± 526 in current study, mean $\pm$ SD from 3 independent experiments). However, we shall also admit that such method shall overestimate the loading of intact GVs, to some extent, considering potential collapse of some GVs during the mixing agitation and loss of free GVs during centrifugal washing.

To evaluate the influences of labeling on NK cells, the cell survival and proliferation after the labeling were examined via MTS assay and transwell assay, where the labeling by microbubble (MB) and their shattered components (MB-S) were also included for comparisons. The labeling procedures were not causing much burden on cell survival as determined by trypan blue exclusion after the handling, where ~90% cells remained viable after all binding procedures in all experiments. The FBS was used as the model attractant to evaluate the migration ability of labeled cells through membranes with 5μm pores (Fig. 1e). The migrated cells were collected and quantified (Fig. 1f). The migration of NK cells bound with either GVs or ruptured MBs was not affected, as no difference in counted migration was observed between these two groups and the control group. While in the MB-labeled group, the number of migrated cells was significantly lower than all other groups, suggesting a compromised migratory ability of NKs bound with MBs. Moreover, the MTS results suggested that the proliferation of labeled cells was not influenced by either GVs or MBs, with no significant difference between the labeled groups and control group (Fig. 1g). As we hypothesized, the traditional contrast agent, MBs, has hamstrung the tagged immune cells from effective migration and infiltration due to their sizes under intact structure. As the effective migratory activities shall be the pre-requisite for executing effector functions in cellular immunotherapy, we proposed to use nanosized GVs for cellular labeling, considering their previously demonstrated stability and effective entry into the tumor [39]. Accompanying the viability assay, the observed migration profile in transwell assay showed effective infiltration of GV-labeled NK cells *in vitro*, compared to non-labeled counterparts or MB-labeled ones, suggesting a potent method for detecting tumor-infiltrating NK cells via ultrasound imaging. Other than the migratory ability that we most concerned, we further examine other functionalities that are related to effector functions of NK cell after accumulation in tumors (Supplementary Fig. S2). Indeed, no significant impact on NK-92 cell functionalities was observed on the mRNA level.

Combining the results above, the compromised migration in MB-labeled group was most likely due to the physical properties of structurally intact MBs, since no noticeable cytotoxicity or bioeffect of MBs was observed. The large sizes of intact MBs attached on cells were highly probable to create extra barriers that hindered the crossing of NKs across the pores, resulting in a reduced number of migrated cells in MB-labeled group. By contrast, the GVs exhibited good biocompatibility with the labeled cells, while imposing no obvious impact on cell functionalities. Such properties are greatly desirable for tracking adoptive immune cells since they are expected to migrate and infiltrate into tumor tissues.

3.2. In vitro *ultrasound imaging properties*

After confirming the binding between GVs and NK cells, we proceeded to evaluate the ultrasound imaging properties of GV-labeled NK cells (GVNK) in agarose phantom wells right after the labeling procedures. Both traditional B-mode images and nCEUS images under nonlinear contrast (NLC) mode were collected for comparison. In traditional B-mode images (Fig. 2a), the control cells without labeling started to show certain level of signal in B-mode images at the density of 10^5 cells/mL and stood out from background at 10^6 cells/mL. However, the control cells did not exhibit any signal in nonlinear contrast mode even at the density up to 10^6 cells/mL. In GVNK group, the similar trend was observed across different densities in B-mode images, while the GV-labeled cells exhibited some level of contrast signal in NLC images at density of 10^5 cells/mL and became considerably bright at 10^6 cells/mL. The contrast signal was lost after applying the high-power bursts in the GVNK group, returning to the similar level with their non-labeled counterparts. The signal intensities in NLC images were further quantified (Fig. 2c). In GVNK group, a slight enhancement was seen when the density reached 10^5 cells/mL, with a dramatic rise from 10^5 cells/mL to 10^6 cells/mL. While as expected, the non-labeled cells showed no noticeable change in NLC intensity w.r.t. increasing cell density. A 2.6-fold enhancement was observed in GV-labeled cells to their non-labeled counterparts at 10^6 cells/mL with statistical significance, indicating a detection threshold around 10^6 cells/mL in current labeling paradigm. The labeling by GVs granted the cells clear contrast signal in nCEUS images, owing to the nonlinear echogenicity of GVs. Either non-labeled cells or biological tissues were echogenic predominantly in fundamental frequency, which hinders the detection of target cell populations by traditional B-mode imaging after adoptive transfer. These current results suggested that the labeling by GVs facilitate the specific detection of labeled cells of interest in biological tissues. In nCEUS imaging, the tissue background is greatly suppressed as they usually do not exhibit nonlinear echogenicity. The GVs, with their well-studied nonlinear echogenicity, would in turns enable specific detection of cells with GVs tethered to their surfaces.

The persistence of the NLC signal after GV-labeling was further evaluated, with the labeled cells imaged after different post-labeling incubation time (Fig. 2b&d) and balanced to the same density. Although the signal intensities dropped with increasing incubation time at 37 °C (Fig. 2d), the labeled cells remained distinguishable from non-labeled cells even after 48 h incubation (Fig. 2b). The significant contrast enhancement was observed for up to 48 h post-labeling incubation, with a return to baseline when imaged at 72 h (Fig. 2d). Such signal decrease was not observed in previous longevity test regarding GVs themselves [39]. We give two speculated reasons that might be leading to the *in vitro* signal loss. Firstly, at each time point examined, the cells were counted and resuspended so that the density was balanced to the same density as the initial one. Considering the cell proliferation during the long incubation period, the rebalancing process might lead to decreased labeling rate, as the total amount of GVs incorporated in the system would remain unchanged while the cell number increased. Secondly, potential cell-GV interactions might also underly the loss of ultrasound signal after the long incubation time. Although spa-

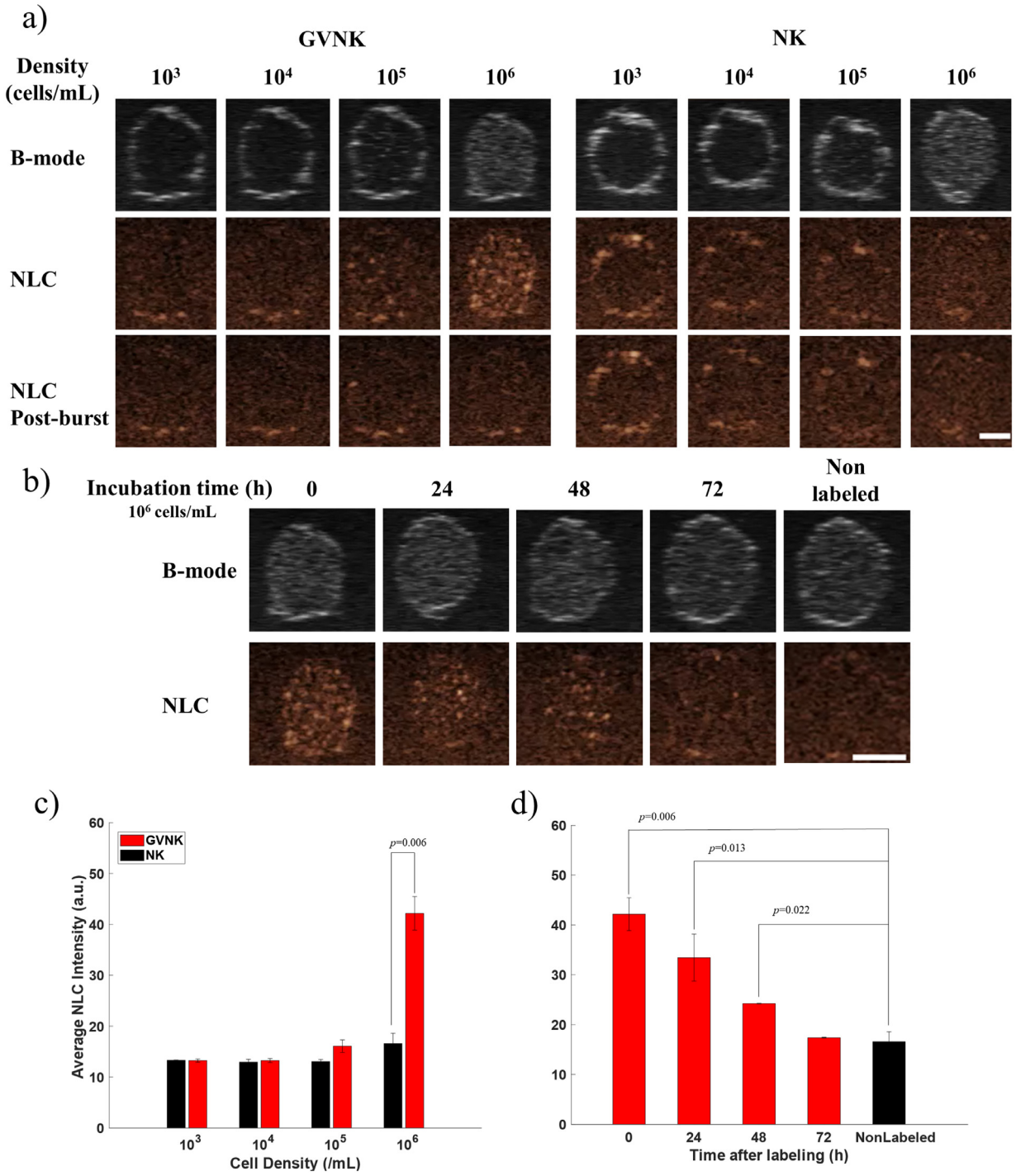

Fig. 2. Ultrasound imaging properties of labeled and non-labeled NK-92 cells *in vitro*. a. The ultrasound images of labeled and non-labeled NK-92 cells at different cell densities under B-mode and NLC mode. b. The ultrasound images of GV-labeled NK-92 cells after different post-labeling incubation time under B-mode and NLC mode, with density balanced at 10^6 cells/mL. Scale bars, 2mm. c, d. Quantification of NLC intensities in a & b. The average intensities were quantified in manually drawn ROIs covering the phantom wells containing cell suspension (n=3, data presented as mean ± SD). Statistical differences were analyzed by one-way analysis of variance (ANOVA) and two-tailed Student's t-test, with statistical differences indicated with corresponding p-values.

tial arms in the biotinylation reagent were introduced to prevent direct contact between cells and GVs, the NK-92 cells are known to cluster during incubation, which introduce chances of GV-cell contact and hence cell-GV interactions. Potentially, some interactions might cause GV structure breakdown, or in certain cases, rupture GVs due to some cell-cell interactions. Nevertheless, with previously reported trafficking and homing dynamics of NK cells [15]. the current signal persistence up to 48 h shall suffice the purpose of early-phase tracking of the adoptive NK cells, as they are expected to infiltrate tumors within hours after infusion.

3.3. In vivo *detection of labeled NK cells in healthy animals*

Upon confirming the *in vitro* ultrasound imaging properties of GV-labeled NK cells, we then evaluated the detectability of GV-labeled NK cells *in vivo*. We first chose the liver as an example

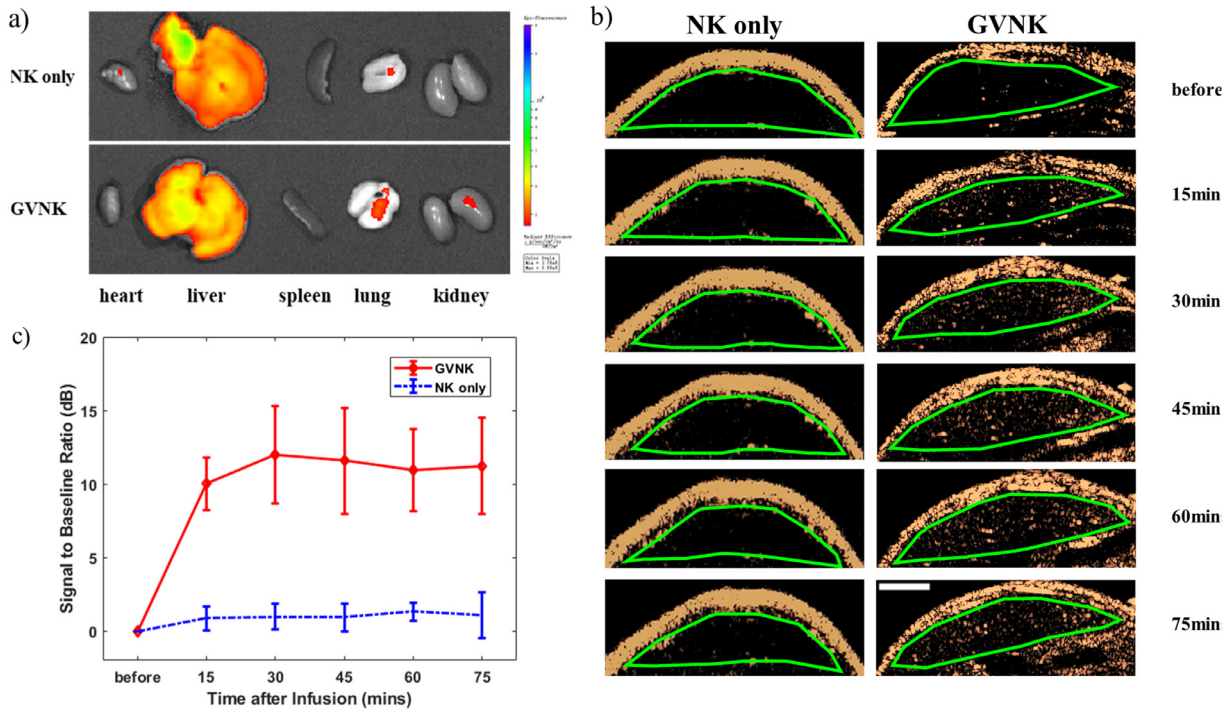

Fig. 3. The detectability of GV-labeled NK-92 cells by ultrasound imaging *in vivo*. a. Representative *ex vivo* IVIS images of major organs collected at 1h after the intravenous injection of non-labeled (NK only) and GV-labeled (GVNK) EGFP-expressing NK-92 cells. Positive fluorescence indicates presence of adoptive NK-92 cells. b. Representative *in vivo* NLC images of mouse livers outlined by ROIs (green line) before and after the infusion of non-labeled (NK only) and GV-labeled (GVNK) NK-92 cells. Scale bar, 2 mm. c. Quantification of NLC intensity changes in b. Average intensities were quantified in manually drawn ROIs covering the liver, and normalized to the baseline intensities before the cell infusion. ($n = 3$, data presented as mean ± SD)

homing environment for the evaluation, as it has been widely reported as one of the major accumulation spots for adoptive NK cells after infusion [15]. In two groups of healthy nude mice, we infused intravenously either GV-labeled (GVNK) or non-labeled (NK only) EGPF-expressing NK-92 cells, at 5×10^6 cells each mouse. One mouse from each group was sacrificed at 60 min after infusion for organ collection and *ex vivo* biodistribution analysis by IVIS imaging (Fig. 3a). The distribution of EGFP intensities indicated a post-infusion accumulation majorly in the liver, 60 min after the adoptive transfer for both groups, as previously reported [15,20,22,23]. The nCEUS ultrasound imaging was conducted on the rest of mice in both groups (Fig. 3b), and the NLC signal intensity changes in the liver were quantified (Fig. 3c). Before the adoptive transfer, the liver exhibited minimal contrast signal under NLC mode compared to the skin surface or tissue boundaries for both groups. After i.v. infusion of the cells, no observable signal enhancement could be observed in the liver for NK-only group, while a clear increase could be seen in the GVNK group (Fig. 3b). The quantification of the NLC intensities suggested a plateau around 10dB enhancement in the liver, reached at 15 min post-infusion and persisted up to 75 min after the infusion of GV-labeled NK cells. At the meantime, no change was observed for the NLC intensities in NK-only group (Fig. 3c). The *ex vivo* fluorescence distribution suggested positive accumulation of adoptive NK cells in both groups, while only those cells tethered with GVs gave rise to NLC in livers for GVNK group. Note that the free GVs have been reported to be degraded in liver through phagolysosomes, which resulted in rapid liver contrast decay and return to baseline within one hour [42]. Different from the degradation dynamics reported before, the contrast dynamics in current study reached the plateau between 15 and 30 min and persisted towards an hour until the mice were sacrificed, unlikely to be contributed by any free GV alone. This indicated that the NK-bound GVs experienced a different degradation process from plain GVs *in vivo*, leading to a longer persistence in terms of structural integrity and hence echogenicity in the liver, allowing the tracking of GV-labeled cells to a longer term. The trace of GV-labeled NK cells in the liver was detected *in vivo* via nCEUS imaging, suggesting a successful ultrasound-based detection of cells in healthy animals by the proposed labeling scheme.

3.4. In vivo *tracking of NK cells for tumor immunotherapy*

As we confirmed the detectability of GV-labeled cells *in vivo*, we now moved forward to the tracking of GV-labeled NK cells in a model of adoptive NK immunotherapy for tumor-bearing mice. The mice received either plain GVs (GV only), PBS, non-labeled NK-92 cells (NK only), or GV-labeled NK-92 cells (GVNK) through i.v. injection. For half of the mice in GV-labeled group, we further administrated a single dose of IL-2 i.p. to boost the activities of infused NK cells (GVNK+IL2). The contrast signal within the tumor was then evaluated via 3D ultrasound scans under NLC mode at several time points after the infusion (Fig. 4a). One mouse from each cell-infused group was sacrificed at 24 h post-infusion for checking the distribution of adoptive cells by *ex vivo* fluorescence imaging (Fig. 4b). Positive fluorescence was observed in tumors for all groups, while the biodistribution in major organs was in general as previously reported [20,23]. With the reported NK cell accumulation at this time point, our *ex vivo* data suggested similarly a positive tumor homing of adoptive NK cells at 24 h post-infusion, without noticeable impact on other major organs.

We further used the ultrasound imaging to monitor the dynamical process of NK cell trafficking and homing to the tumor after adoptive transfer. As shown in the single-slice images, the intra-tumoral tissues exhibited only a low level of NLC signal in all groups before the infusion (Fig. 4c). Such baseline contrast signal should be due to the high heterogeneity presented in tumor tissues, whereas the tissue background was still greatly

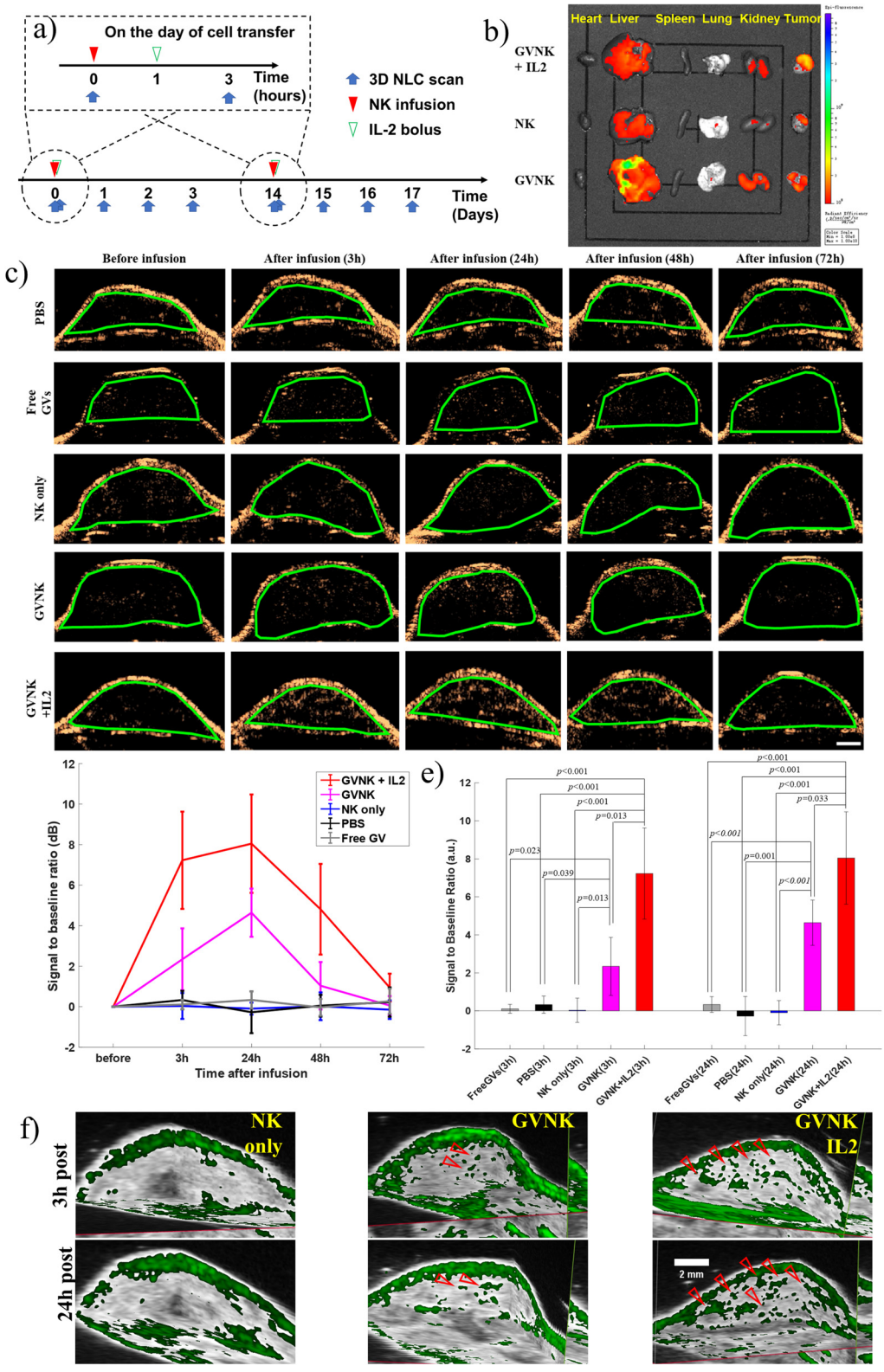

Fig. 4. *In vivo* ultrasound tracking of GV-labeled NK-92 cells in tumor-bearing mice. a. Graphical summary of the experimental timeline. After the tumor size reached the criteria (day 0), the mice received two doses of treatment at day 0 and day 14, respectively. The 3D ultrasound scans were performed before and at 3, 24, 48 and 72 h after the i.v. infusion of either NK-92 cells (GVNK+IL2, GVNK, NK-only), free GVs or PBS. For the group of mice receiving IL-2 co-treatment, the IL-2 was intraperitoneally injected at 1h following the cell infusion. b. Representative *ex vivo* IVIS images of major organs and tumors collected at 24h after the treatment. Positive fluorescence indicates the presence of adoptive NK-92 cells. c. Representative *in vivo* NLC images of the tumor outlined by ROIs (green line) before and after the treatment. Scale bar, 2mm. d. The average NLC intensities were quantified by manually drawn ROIs covering the intra-tumoral tissues through the 3D scans, with the changes normalized to baseline intensities obtained before the infusion (3 animals for each group, 2 repeats in each animal, 6 repeats in total for each point. Data presented as mean ± SD). e. Comparisons and statistical differences of average intra-tumoral contrast intensity changes at 3h and 24 h post-infusion. Statistical analysis was performed by ANOVA test, with statistical differences indicated by corresponding p-values. f. Representative images of 3D ultrasound scans of tumors at 3 h and 24 h after the cell infusion, red triangles indicate the spots of contrast enhancement compared to baseline.

suppressed under NLC mode, facilitating the specific detection of tumor-homing adoptive cells upon contrast enhancement. As in the liver imaging results, the non-labeled NK cells did not contribute to any noticeable change in the scan at all time points following the transfer. Similar patterns could be observed in the scans for PBS and GV-only groups (Fig. 4c), where no change was seen across all post-infusion scans. By contrast, clear spot-like enhancement could be observed in both GVNK and GVNK+IL2 groups following the infusion of labeled NK cells. The enhanced NLC signal in these two groups was observed to decrease around 48h and returned to baseline level at 72 h post-infusion. The average NLC intensities were quantified across slices in the whole tumor volume and normalized to the baseline NLC intensity measured before infusion (Fig. 4d&e). By comparing the intra-tumoral contrast, significant differences were seen in both groups with GV-labeling (GVNK, GVNK+IL2) compared to control groups at both 3 h and 24 h post-infusion (Fig. 4e). Significant increase in the intra-tumoral NLC intensities could be seen in the GV-labeled groups as early as 3 h post-infusion, with a sustained enhancement up to 24 h. Similar to the observations on single-slice images, minimal changes were observed for NK-only, PBS and GV-groups. Combining with our *ex vivo* data indicating positive NK cell accumulation in tumors (Fig. 4b), the traces of tumor-homing NK cells were detected by ultrasound imaging with GV-labeling. The cell-tethered GVs with nonlinear echogenicity enabled detection of the tumor-homing NK cells under nCEUS imaging. The early-phase tumor recruitment of adoptive NK cells at 3 h post-infusion was also reported by previous optical imaging studies, while a similar detection was made in current study using ultrasound imaging. After the infusion of GV-labeled NK-92 cells, a 2.3dB increase of intra-tumoral contrast was recorded in GVNK group at 3 h post-infusion, which continued to rise to a peak around 4.6dB at 24 h as increasing number of labeled NK cells infiltrated the tumor (Fig. 4d&e, magenta). The signal started to decrease after 24 h as the average NLC intensity dropped at 48 h and returned to baseline at 72 h, which should be related to the signal decay of cell bound GVs as observed *in vitro*. The 3D-resonstructed contrast mapping also suggested obvious intra-tumoral contrast enhancement in the labeled groups as early as 3 h post-infusion (Fig. 4f). The enhancement was localized to several spots in the tumor instead of any wide-spread pattern, which should be related to the spatial heterogeneity of the intratumoral immune cell recruitment [18]. The spots with enhancement further increased in number and sizes in the reconstructed maps at 24 h both in GVNK and GVNK+IL2 groups, consistent with the observed changes in single-slice imaging (Fig. 4f).

As the IL-2 has been widely employed for boosting the activities and survival of adoptive immune cells like NK cells [43], we further employed the IL-2 adjuvant in form of a single i.p. bolus injection in 3 mice at 1h following the infusion of GV-labeled NK cells, so that the active tumor targeting of the infused cells would be promoted during their post-infusion trafficking. As expected, stronger ultrasound contrast was observed for GVNK+IL2 group both in single-slice and 3D-reconstructed images (Fig. 4c&f). Prominent bright spots could be seen in single-slice images both at 3 h and 24 h post-infusion in GVNK+IL2 group, with a wider-spread pattern in the tumor tissue. A 7dB rise of overall intratumoral NLC intensity was seen at 3h in GVNK+IL2 group, significantly higher than that in GVNK group, indicating an increased trafficking and recruitment of labeled NK cells to the tumor site (Fig. 4d&e, red). Considering the serum half-life of i.p. administrated IL-2, the booster effects of the bolus applied in current study should be presented for a few hours during the early post-infusion phase of NK cells [44]. Indeed, the NLC increase rate was slower during 3∼24h in GVNK+IL2 group, with a near 8dB peak presented at 24 h, while still being significantly stronger than GVNK group (Fig. 4d, red). The decrease trend after 24h in GVNK+IL2 group was similar to that in GVNK group, which suggested a similar mechanism of GV signal decay in the two groups.

3.5. Tumor slices

To further confirm the presence of adoptive NK cells within the tumor and co-validate the ultrasound imaging results, we harvested one tumor from each group at 24 h post-infusion for analysis with fluorescence microscopy. Positive EGFP fluorescence was seen in all groups receiving NK-92 transfer (NK-only, GVNK, GVNK+IL2) in the confocal images of tumor slices (Fig. 5a). There was positive GV fluorescence only in groups where GVs were tethered to NK cell surfaces (GVNK, GVNK+IL2), which also showed colocalization with EGFP signal in these slices (Supplementary Fig. S3). No red fluorescence was observed in the group receiving free GV infusion as expected. In our previous study on molecular ultrasound imaging by GVs, we have examined the dynamics of free GVs without tumor targeting or reticuloendothelial system (RES) escape modifications [39]. Indeed, GVs have been reported to be quickly cleared from bloodstream within 2 h following i.v. infusion [45], which prevents effective extravasation into the tumor tissue. Even with tumor-targeted modifications, those GVs without surface PEGylation experienced rapid clearance within 12 h post-infusion, with no observable GVs from tumor slices collected at 12 h post-infusion [39]. In current study, the SA coating was only introduced for binding with biotinylated cell surfaces, which shall show minimal affinity to tumor tissues. Therefore, it is not surprising to observe no red fluorescence in tumor slices collected at 24 h post-infusion in current study. This eased the complications of observing any signal originating from free contrast agents instead of the labeled NK cells during nCEUS imaging. Considering the colocalization profile observed in the slices, and that NLC changes were only observed in GVNK and GVNK+IL2 groups, the results suggest successful detection of tumor-infiltrating NK-92 cells after the adoptive transfer, where the cell-bound GVs were contributing to the ultrasound contrast signal.

By quantifying the $EGFP^+$ cells in the field, no noticeable difference was seen between the number of NK cells in NK-only and GVNK groups (Fig. 5b), suggesting a similar cellular trafficking to tumors of GV-labeled NK cells comparing to their non-labeled counterparts. This is consistent with our observations *in vitro*, where GV-based labeling did not impose any noticeable burden on cellular migration and infiltration. The GVNK+IL2 showed significantly larger number of $EGFP^+$ cells in the field than the other two groups with cell transfer (Fig. 5b), consistent with the well-established effects of IL-2 on boosting NK-92 cell trafficking. With the same labeling rate achieved during the *ex vivo* labeling protocol, the increased ultrasound contrast intensities were correlated to the increased number of tumor-homing adoptive NK-92 cells with GV labeling. This suggests a successful monitoring of cellular trafficking dynamics to the tumor by the proposed strategy, when the NK cell-based immunotherapy was applied synergically with IL-2 supplementation.

4. Discussions

Noninvasive cell tracking techniques, thanks to recent advances in imaging tools and biomaterials, have enabled the *in vivo* monitoring of the trafficking, accumulation and functionalities of specific cell population in living organisms. The recent decades have seen their tremendous contributions in basic biological research as well as the development of cell-based immunotherapies. In this study, we demonstrated for the first time the successful tracking of adoptive NK cells by ultrasound imaging following systemic administration, labeled with biogenic nUCAs, in a xenograft model of hepatocellular carcinoma. The successful labeling of NK-92 cells

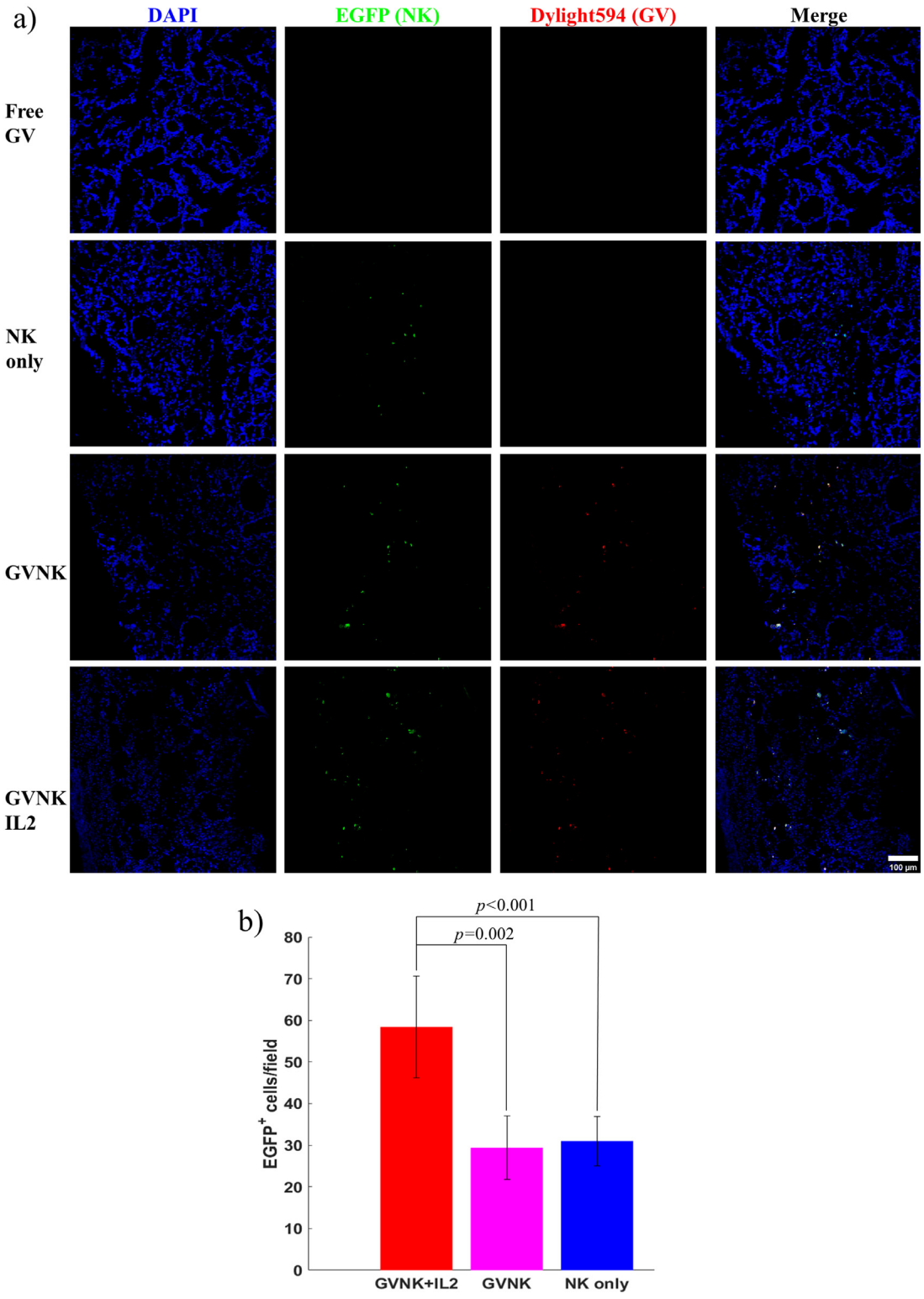

Fig. 5. Fluorescence microscopy of tumor slices. a. Representative fluorescence microscopy of tumor slices collected at 24 h after the infusion of free GV, non-labeled NK cells (NK only), GV-labeled NK cells (GVNK), labeled NK cells with IL-2 co-treatment (GVNK+IL2). The presence of adoptive NK-92 cells was indicated by the EGFP fluorescence (green), with the Dylight594 (red) signal indicating the presence of GVs. Colocalization of NK cells and GVs were presented in GVNK and GVNK+IL2 groups. b. Quantification of EGFP+ cells per field in the tumor slices in all groups treated with adoptive NK-92 transfer. Cell number counted in slices from each mouse, 3 mice for each group, with significant differences indicated by corresponding p-values (Data presented as mean ± SD).

by GVs were demonstrated *in vitro*, enabling specific and sensitive detection of the labeled cells under nCEUS imaging, without noticeable impact on cell viability or migration ability. The tracking strategy was further applied for monitoring adoptive NK cell immunotherapy on tumor-bearing mice. Via nCEUS scans at multiple points after the infusion, we identified the early-phase trafficking of adoptive NK-92 to the tumor as early as 3h post-infusion, with a sustained accumulation up to 24h, with the presence of tumor-infiltrating adoptive cells co-validated by *ex vivo* optical imaging methods. Furtherly, we showed that the proposed tracking strategy was capable of noninvasively monitoring the boosted trafficking of adoptive NK cells to the tumor, actively promoted by a bolus injection of IL-2 after cell transfer.

With the observed signal decay between 24 and 48 h after labeling *in vitro*, as well as a previously reported similar decay of targeted GVs in tumor microenvironment [39], the cell-GV interactions might also be a possible mechanism underlying the breakdown of GVs and hence loss of ultrasound signal over time *in vivo*. Moreover, in this study, we designed the experiments centering around examining the capability of the proposed strategy on tracking adoptive immune cells during their trafficking to tumors. We focused on the early-phase trafficking dynamics of the adoptive NK cells. By the proposed tracking strategy, we managed to noninvasively monitor the early-phase trafficking of adoptive NK cells to the tumor. With a single-dose administration of IL-2 after cell transfer, which has been known to quickly increase the adoptive NK cell trafficking to tumors, we observed significant increase in NLC intensities 3 h and 24 h post-infusion. The contrast enhancement was consistent with increased number of NK cells observed in tumor slices, indicating a rapid elevation of the tumor recruitment of adoptive NK cells, successfully tracked via ultrasound imaging of these GV-labeled cellular targets. The proposed strategy and the recorded early-phase trafficking profiles provide valuable information for monitoring and optimization of adoptive NK cell immunotherapy, indicating factors to be considered when designing assistive interventions for improving the therapeutic outcomes. At the meantime, the NK-92 cells are known to rely on continuous IL-2 supplementation to maintain their viability and cytotoxicity [46]. However, we applied only a single dose of IL-2 bolus in GVNK+IL2 group, leaving GVNK and NK-only groups un-supplied to set baseline trafficking status for comparisons. Neither did we apply any follow-up supplementation within the ultrasound imaging window (72 h), in order to avoid confounding changes in the trafficking dynamics. As the viability NK-92 cells were known to diminish quickly after withdrawal of IL-2 supplementation, the cell membrane-bound GVs might be cleared out together with the cell debris in the tumor by resident cells in TME, contributing another possible signal decay mechanism *in vivo*. We shall admit that the single IL-2 bolus applied in our study should indeed be insufficient to alter the therapeutic effect significantly, neither should it be adequate to maintain NK-92 cell viability for long. However, the *in vitro* functional characterizations of labeled NK cells, in turns, suggested competent NK cell viability and functionalities upon GV labeling, which are believed to deliver promising therapeutic effects if fully supplemented. We shall leave the in-depth study and optimization of the therapeutic effect, as well as its relationship to the observed trafficking dynamics by ultrasound tracking strategy to our future studies.

Moreover, we demonstrated the feasibility of monitoring early-phase tumor recruitment of adoptive cells via the ubiquitous ultrasound imaging, which is a cost-effective and readily accessible in most clinical settings. The real-time imaging compatibility of ultrasound imaging also indicates potentials of combining proposed tracking strategy with image-guided interventions. Specifically, the ultrasound has been shown in recent years as a reliable physical intervention method, capable of delivering mechanical energy noninvasively for modulating immune cell activities [47,48]. With the tracking strategy demonstrated in current paper, we see great potentials in implementing ultrasound-guided ultrasound control of adoptive immune cell functionalities in the future. The practical application and management of ACT would be much benefited by such versatile and already-on board imaging technique. A more detailed investigation on the contrast signal profile w.r.t. cell density, labeling time, as well as corresponding pharmacokinetics of adoptive cells, shall further contribute to quantitative tracking in ACT via ultrasound imaging. The exploration of nanosized contrast agents with clinically approved composition would also accelerate the translation of such tracking strategy.

Some previous studies have touched the ultrasound imaging of cellular targets [49–51], yet there is still a lack of strategy for ultrasound-based tracking of systematically infused immune cells with effector functions. Cationic MBs have been employed for neural progenitor cell labeling, which enabled the detection of the MB-loaded cells in liver by nCEUS imaging *in vivo*, suggesting the feasibility of ultrasound-based tracking of cellular targets [49]. However, the labeling by MBs was inherently incompatible with tracking in ACT, where the compromised cell migration ability was undesired. In another recent attempt relying on micron-sized UCAs, NK cells conjugated with sonazoid MBs were intratumorally injected and imaged with ultrasound [51]. Although the results indicated the detectability of UCA-labeled immune cells in tumor tissues, the fundamental incompatibility of micron-sized UCA labeling with systematically infused immune cells was not addressed. With the shifting of focus on nano-sized contrast agents, porous silica nanoparticles encapsulating drug payload and phase transformable perfluorocarbon was developed for image-guided drug delivery [50]. These nanoparticle-loading macrophages would exhibit low level of echogenicity *in vivo* due to partial vaporization of the perfluorocarbon, allowing temporary detection of carrier cells after infusion or one-time detection upon high-intensity ultrasound burst. The loss of echogenicity was at a similar rate to traditional contrast agents, while the burst-based detection was destructive to the cells, undesired for tracking in ACT.

In current study, we employed the biogenic nano-sized contrast agents, GVs, with high stability and biocompatibility, with which the ultrasound imaging-based tracking of NK cells could be achieved following systematic transfer. We adopted an *ex vivo* direct labeling of the NK-92 cell with GVs via biotin-streptavidin conjugation, which allows labeling of a wide-spectrum of non-phagocytic lymphocytes with low cost. Therefore, the proposed ultrasound tracking strategy should be applicable to not only adoptive NK, but also other immune cells like cytotoxic T cells in cell-based immunotherapies. The labeling with nanosized contrast agents showed no noticeable impact on cell viability and migration ability *in vitro*, and the tumor infiltration was unaffected as expected. Although such direct labeling strategy enjoys the cost-effectiveness and ease of use, it is also subject to limitations in monitoring timespan and scope. Both cell-marker interactions and cell expansion *in vivo* could lead to signal decay, hindering the tracking of labeled cells for a longer term. The signal originating from cell-bound contrast agents contributes information on their whereabouts, while the actual viability or activation status of these cells would be hard to assess. Indeed, the surface attachment of contrast agents might also impose certain level of steric hindrance during the binding between effector cells and tumor cells, if presented in bulk. These encourage an intracellular labeling strategy with nanosized contrast agents, preferably genetical encoding that could be tethered to cellular fate. Fortunately, GVs, as biogenic protein structures, have been reported as genetically encodable reporters for ultrasound imaging, with several initial demonstrations on GV-expressing mammalian cells [37,38]. While the stable expression of GVs in mammalian cells remained challenging in

acoustic reporter gene technology, immune cells also feature complex intracellular environment that might compromise GV assembly. With immune cell-compatible GV gene clusters, the spectrum of monitoring would be expanded to not only trafficking dynamics, but also longer-term cell survival as well as activation status with prognosis relevance [12]. Moreover, efforts were seen in recent years on the iterations of the acoustic reporter gene and corresponding imaging schemes, enabling detection of these biogenic nUCAs with higher specificity and sensitivity [33,38,40]. With the demonstrated feasibility of tracking GV-labeled immune cells by ultrasound imaging, we expect tremendous opportunities in this field for longer-term and functional immune cell tracking, as well as image-guided biopsy for in-depth investigation of the TME remodeling upon the retention of adoptive immune cells. Hence, the current study also encourages further optimization of acoustic reporter genes, and the related use in ultrasound-based longitudinal immune cell tracking for extended purposes.

The leakage of markers is also another major concern on direct labeling approaches in cell tracking, where the efflux of labeling agents might cause altered distribution and misinterpretation in the imaging results. We would expect this to be less of a concern in the proposed strategy. We chose the biotin-streptavidin conjugation method in current study for attaching GVs on the surface of NK-92 cells, which is the one of the strongest non-covalent interactions in nature. The bond remains stable even under extreme conditions (temperature, pH, de-naturing agents, etc.) once formed, which has been extensively used for functional decorations of molecules or particles at various scales [52]. The interaction has also been exploited for labeling and tracking biotinylated cytotoxic T lymphocytes, with high labeling efficiency and stability demonstrated for imaging probes of various types including optical, magnetic and radioactive tracers, without influence on cell viability of functionality [53]. Therefore, the attachment of intact GVs on NK cells is expected also remain stable during blood circulation, and we indeed observed no noticeable presence of free GVs in tumor slices collected in groups with GV-labeled NK cell infusion. Nevertheless, the detach of GV shells from labeled cells, most probably due to loss of structural integrity, will not contribute to signal generation in organs related to their degradation, as the structural integrity of GVs is critical for their echogenicity in ultrasound imaging. However, such potential collapse shall limit the highest contrast enhancement achievable in the ultrasound imaging. It is thus a meaningful pursuit in future studies to improve the stability of nUCAs to avoid unwanted burst at *in vivo* conditions. The free GVs also experience quick degradation in the liver with the loss of their hollow-shell structure [42], reducing the chance of undesired contrast enhancement in organs without actual accumulation of the target cells. We also encourage a more in-depth monitoring of the contrast dynamic changes in other organs, by which the specificity of the GV-based labeling and ultrasound tracking shall be investigated.

5. Conclusions

In conclusion, this study demonstrated the capacity of ultrasound imaging to noninvasively monitor adoptive NK-92 cell trafficking in cellular immunotherapy. We were further able to identify the dynamical changes in tumor recruitment of adoptive cells boosted by early-phase IL-2 bolus, providing indications for related treatment strategy design and optimization in NK cell immunotherapies. With the demonstrated compatibility of the ubiquitous ultrasound imaging tool with the tracking of therapeutic cells, cell-based immunotherapeutic strategies would enjoy the advantages offered by ultrasound imaging, providing extra information for making treatment-related decisions at earlier stage after the treatment, with appealing potentials in clinical applications.

Declaration of Competing Interest

The authors declare that they have no known competing financial interests or personal relationships that could have appeared to influence the work reported in this paper.

Acknowledgment

This work was supported by the Hong Kong Research Grants Council General Research Fund (15104520), Hong Kong Innovation Technology Fund (MRP/018/18X and MHP/014/19), Shenzhen-Hong Kong-Macau Science and Technology Program (SGDX20201103095400001), internal funding from the Hong Kong Polytechnic University Research Institute of Smart Ageing (1-CD76) and Hong Kong Polytechnic University (1-ZVW8). The authors would like to thank the facility and technical support from the University Research Facility in Life Sciences (ULS) of The Hong Kong Polytechnic University.

Supplementary materials

Supplementary material associated with this article can be found, in the online version, at doi:10.1016/j.actbio.2023.07.058.

References

[1] J.N. Brudno, J.N. Kochenderfer, Chimeric antigen receptor T-cell therapies for lymphoma, Nat. Rev. Clin. Oncol. 15 (1) (2018) 31–46.
[2] J.S. Miller, Therapeutic applications: natural killer cells in the clinic, Hematology 2013 (1) (2013) 247–253 the American Society of Hematology Education Program.
[3] A.D. Waldman, J.M. Fritz, M.J. Lenardo, A guide to cancer immunotherapy: from T cell basic science to clinical practice, Nat. Rev. Immunol. 20 (11) (2020) 651–668.
[4] C.L. Bonifant, H.J. Jackson, R.J. Brentjens, K.J. Curran, Toxicity and management in CAR T-cell therapy, Mol. Ther. Oncolytics 3 (2016) 16011.
[5] S. Kakarla, S. Gottschalk, CAR T cells for solid tumors: armed and ready to go? Cancer J. 20 (2) (2014) 151.
[6] M. Shevtsov, G. Multhoff, Immunological and translational aspects of NK cell-based antitumor immunotherapies, Front. Immunol. 7 (2016) 492.
[7] M.J. Pittet, J. Grimm, C.R. Berger, T. Tamura, G. Wojtkiewicz, M. Nahrendorf, P. Romero, F.K. Swirski, R. Weissleder, *In vivo* imaging of T cell delivery to tumors after adoptive transfer therapy, Proc. Natl Acad. Sci. 104 (30) (2007) 12457–12461.
[8] S. Krebs, M.M. Dacek, L.M. Carter, D.A. Scheinberg, S.M. Larson, CAR Chase, Where do engineered cells go in humans? Front. Oncol. 10 (2020) 577773.
[9] M. Varani, S. Auletta, A. Signore, F. Galli, State of the art of natural killer cell imaging: a systematic review, Cancers 11 (7) (2019) 967.
[10] S. Maddineni, J.L. Silberstein, J.B. Sunwoo, Emerging NK cell therapies for cancer and the promise of next generation engineering of iPSC-derived NK cells, J. Immunother. Cancer 10 (5) (2022).
[11] J.A. Myers, J.S. Miller, Exploring the NK cell platform for cancer immunotherapy, Nat. Rev. Clin. Oncol. 18 (2) (2021) 85–100.
[12] A. Volpe, P.S. Adusumilli, H. Schöder, V. Ponomarev, Imaging cellular immunotherapies and immune cell biomarkers: from preclinical studies to patients, J. Immunother. Cancer 10 (9) (2022) e004902.
[13] M. Gerwing, K. Herrmann, A. Helfen, C. Schliemann, W.E. Berdel, M. Eisenblätter, M. Wildgruber, The beginning of the end for conventional RECIST—novel therapies require novel imaging approaches, Nat. Rev. Clin. Oncol. 16 (7) (2019) 442–458.
[14] K.V. Keu, T.H. Witney, S. Yaghoubi, J. Rosenberg, A. Kurien, R. Magnusson, J. Williams, F. Habte, J.R. Wagner, S. Forman, Reporter gene imaging of targeted T cell immunotherapy in recurrent glioma, Sci. Transl. Med. 9 (373) (2017) eaag2196.
[15] M. Shapovalova, S.R. Pyper, B.S. Moriarity, A.M. LeBeau, The molecular imaging of natural killer cells, Mol. Imaging 17 (2018) 1536012118794816.
[16] M.R. Weist, R. Starr, B. Aguilar, J. Chea, J.K. Miles, E. Poku, E. Gerdts, X. Yang, S.J. Priceman, S.J. Forman, PET of adoptively transferred chimeric antigen receptor T cells with 89Zr-oxine, J. Nucl. Med. 59 (10) (2018) 1531–1537.
[17] F. Galli, M. Varani, C. Lauri, G.G. Silveri, L. Onofrio, A. Signore, Immune cell labelling and tracking: implications for adoptive cell transfer therapies, EJNMMI Radiopharm. Chem. 6 (1) (2021) 1–19.
[18] M.F. Kircher, J.R. Allport, E.E. Graves, V. Love, L. Josephson, A.H. Lichtman, R. Weissleder, *In vivo* high resolution three-dimensional imaging of antigen-specific cytotoxic T-lymphocyte trafficking to tumors, Cancer Res. 63 (20) (2003) 6838–6846.
[19] F. Galli, A.S. Rapisarda, H. Stabile, G. Malviya, I. Manni, E. Bonanno, G. Piaggio, A. Gismondi, A. Santoni, A. Signore, *In vivo* imaging of natural killer cell trafficking in tumors, J. Nucl. Med. 56 (10) (2015) 1575–1580.

[20] L. Zhu, X.J. Li, S. Kalimuthu, P. Gangadaran, H.W. Lee, J.M. Oh, S.H. Baek, S.Y. Jeong, S.W. Lee, J. Lee, Natural killer cell (NK-92MI)-based therapy for pulmonary metastasis of anaplastic thyroid cancer in a nude mouse model, Front. Immunol. 8 (2017) 816.
[21] R. Meier, D. Golovko, S. Tavri, T.D. Henning, C. Knopp, G. Piontek, M. Rudelius, P. Heinrich, W.S. Wels, H. Daldrup-Link, Depicting adoptive immunotherapy for prostate cancer in an animal model with magnetic resonance imaging, Magn. Reson. Med. 65 (3) (2011) 756–763.
[22] N. Sato, K. Stringaris, J.K. Davidson-Moncada, R. Reger, S.S. Adler, C. Dunbar, P.L. Choyke, R.W. Childs, *In vivo* tracking of adoptively transferred natural killer cells in rhesus macaques using 89Zirconium-oxine cell labeling and PET imaging, Clin. Cancer Res. 26 (11) (2020) 2573–2581.
[23] S. Tavri, P. Jha, R. Meier, T.D. Henning, T. Müller, D. Hostetter, C. Knopp, M. Johansson, V. Reinhart, S. Boddington, Optical imaging of cellular immunotherapy against prostate cancer, Mol. Imaging 8 (1) (2009) 7290.2009. 00002.
[24] K. Seitz, D. Strobel, A milestone: approval of CEUS for diagnostic liver imaging in adults and children in the USA, Ultraschall Med. 37 (03) (2016) 229–232 European Journal of Ultrasound.
[25] K. Ferrara, R. Pollard, M. Borden, Ultrasound microbubble contrast agents: fundamentals and application to gene and drug delivery, Annu. Rev. Biomed. Eng. 9 (2007) 415–447.
[26] H. Maeda, The enhanced permeability and retention (EPR) effect in tumor vasculature: the key role of tumor-selective macromolecular drug targeting, Adv. Enzym. Regul. 41 (1) (2001) 189–207.
[27] H. Mulvana, E. Stride, J.V. Hajnal, R.J. Eckersley, Temperature dependent behavior of ultrasound contrast agents, Ultrasound Med. Biol. 36 (6) (2010) 925–934.
[28] H. Shekhar, N.J. Smith, J.L. Raymond, C.K. Holland, Effect of temperature on the size distribution, shell properties, and stability of Definity®, Ultrasound Med. Biol. 44 (2) (2018) 434–446.
[29] M.G. Shapiro, P.W. Goodwill, A. Neogy, M. Yin, F.S. Foster, D.V. Schaffer, S.M. Conolly, Biogenic gas nanostructures as ultrasonic molecular reporters, Nat. Nanotechnol. 9 (4) (2014) 311–316.
[30] A. Lakshmanan, G.J. Lu, A. Farhadi, S.P. Nety, M. Kunth, A. Lee-Gosselin, D. Maresca, R.W. Bourdeau, M. Yin, J. Yan, Preparation of biogenic gas vesicle nanostructures for use as contrast agents for ultrasound and MRI, Nat. Protoc. 12 (10) (2017) 2050–2080.
[31] A. Lakshmanan, A. Farhadi, S.P. Nety, A. Lee-Gosselin, R.W. Bourdeau, D. Maresca, M.G. Shapiro, Molecular engineering of acoustic protein nanostructures, ACS Nano 10 (8) (2016) 7314–7322.
[32] D. Maresca, A. Lakshmanan, A. Lee-Gosselin, J.M. Melis, Y.L. Ni, R.W. Bourdeau, D.M. Kochmann, M.G. Shapiro, Nonlinear ultrasound imaging of nanoscale acoustic biomolecules, Appl. Phys. Lett. 110 (7) (2017) 073704.
[33] D. Maresca, D.P. Sawyer, G. Renaud, A. Lee-Gosselin, M.G. Shapiro, Nonlinear X-wave ultrasound imaging of acoustic biomolecules, Phys. Rev. X 8 (4) (2018) 041002.
[34] X. Hou, Z. Qiu, Q. Xian, S. Kala, J. Jing, K.F. Wong, J. Zhu, J. Guo, T. Zhu, M. Yang, L. SUN, Precise ultrasound neuromodulation in a deep brain region using nano gas vesicles as actuators, Adv. Sci. 8 (21) (2021) 2101934.
[35] L. Song, X. Hou, K.F. Wong, Y. Yang, Z. Qiu, Y. Wu, S. Hou, C. Fei, J. Guo, L. Sun, Gas-filled protein nanostructures as cavitation nuclei for molecule-specific sonodynamic therapy, Acta Biomater. 136 (2021) 533–545.
[36] L. Song, G. Wang, X. Hou, S. Kala, Z. Qiu, K.F. Wong, F. Cao, L. Sun, Biogenic nanobubbles for effective oxygen delivery and enhanced photodynamic therapy of cancer, Acta Biomater. 108 (2020) 313–325.
[37] A. Farhadi, G.H. Ho, D.P. Sawyer, R.W. Bourdeau, M.G. Shapiro, Ultrasound imaging of gene expression in mammalian cells, Sci. Transl. Med. 365 (6460) (2019) 1469–1475.
[38] D.P. Sawyer, A. Bar-Zion, A. Farhadi, S. Shivaei, B. Ling, A. Lee-Gosselin, M.G. Shapiro, Ultrasensitive ultrasound imaging of gene expression with signal unmixing, Nat. Methods 18 (8) (2021) 945–952.
[39] G. Wang, L. Song, X. Hou, S. Kala, K.F. Wong, L. Tang, Y. Dai, L. Sun, Surface–modified GVs as nanosized contrast agents for molecular ultrasound imaging of tumor, Biomaterials 236 (2020) 119803.
[40] R.C. Hurt, M.T. Buss, M. Duan, K. Wong, M.Y. You, D.P. Sawyer, M.B. Swift, P. Dutka, P. Barturen-Larrea, D.R. Mittelstein, Genomically mined acoustic reporter genes for real-time *in vivo* monitoring of tumors and tumor-homing bacteria, Nat. Biotechnol. 41 (2023) 919–931.
[41] Y. Yang, Z. Qiu, X. Hou, L. Sun, Ultrasonic characteristics and cellular properties of Anabaena gas vesicles, Ultrasound Med. Biol. 43 (12) (2017) 2862–2870.
[42] B. Ling, J. Lee, D. Maresca, A. Lee-Gosselin, D. Malounda, M.B. Swift, M.G. Shapiro, Biomolecular ultrasound imaging of phagolysosomal function, ACS Nano 14 (9) (2020) 12210–12221.
[43] R.W. Childs, M. Carlsten, Therapeutic approaches to enhance natural killer cell cytotoxicity against cancer: the force awakens, Nat. Rev. Drug Discov. 14 (7) (2015) 487–498.
[44] M.A. Cheever, J.A. Thompson, D.E. Kern, P. Greenberg, Interleukin 2 (IL 2) administered *in vivo*: influence of IL 2 route and timing on T cell growth, J. Immunol. 134 (6) (1985) 3895–3900.
[45] J. Le Floc'h, A. Zlitni, H.A. Bilton, M. Yin, A. Farhadi, N.R. Janzen, M.G. Shapiro, J.F. Valliant, F.S. Foster, *In vivo* biodistribution of radiolabeled acoustic protein nanostructures, Mol. Imaging Biol. 20 (2018) 230–239.
[46] J.H. Gong, G. Maki, H.G.J.L. Klingemann, Characterization of a human cell line (NK-92) with phenotypical and functional characteristics of activated natural killer cells, 8(4) (1994) 652-658.
[47] Y. Wu, Y. Liu, Z. Huang, X. Wang, Z. Jin, J. Li, P. Limsakul, L. Zhu, M. Allen, Y. Pan, Control of the activity of CAR-T cells within tumours via focused ultrasound, Nat. Biomed. Eng. 5 (11) (2021) 1336–1347.
[48] Y. Pan, S. Yoon, J. Sun, Z. Huang, C. Lee, M. Allen, Y. Wu, Y.J. Chang, M. Sadelain, K.K. Shung, Mechanogenetics for the remote and noninvasive control of cancer immunotherapy, Proc. Natl. Acad. Sci. 115 (5) (2018) 992–997.
[49] W. Cui, S. Tavri, M.J. Benchimol, M. Itani, E.S. Olson, H. Zhang, M. Decyk, R.G. Ramirez, C.V. Barback, Y. Kono, Neural progenitor cells labeling with microbubble contrast agent for ultrasound imaging *in vivo*, Biomaterials 34 (21) (2013) 4926–4935.
[50] Z. Xu, H. Liu, H. Tian, F. Yan, Real-time imaging tracking of engineered macrophages as ultrasound-triggered cell bombs for cancer treatment, Adv. Funct. Mater. 30 (14) (2020) 1910304.
[51] H.W. Song, H.S. Lee, S.J. Kim, H.Y. Kim, Y.H. Choi, B. Kang, C.S. Kim, J.O. Park, E. Choi, Sonazoid-conjugated natural killer cells for tumor therapy and real–time visualization by ultrasound imaging, Pharmaceutics 13 (10) (2021) 1689.
[52] X. Ma, X. Liang, Y. Li, Q. Feng, K. Cheng, N. Ma, F. Zhu, X. Guo, Y. Yue, G. Liu, Modular-designed engineered bacteria for precision tumor immunotherapy via spatiotemporal manipulation by magnetic field, Nat. Commun. 14 (1) (2023) 1606.
[53] A. Li, Y. Wu, J. Linnoila, B. Pulli, C. Wang, M. Zeller, M. Ali, G.K. Lewandrowski, J. Li, B. Tricot, Surface biotinylation of cytotoxic T lymphocytes for *in vivo* tracking of tumor immunotherapy in murine models, Cancer Immunol. Immunother. 65 (2016) 1545–1554.